Vehicle Description Form

(HPVC Form 6)

Human Powered Vehicle Challenge 2011

East Event Host: Rose-Hulman Institute of Technology, Indianapolis, IN. Apr 29-May 1, 2011

West Event Host: Montana State University, Bozeman, MT. May 13-15

http://www.asme.org/hpv

*** *This is a required document for all teams. Please incorporate it into your Design Report* ***

EAST March 28, 2011 | *** *Please Observe Your Due Dates* *** | **WEST** April 11, 2011

Vehicle Description

Competition Location: Indianapolis, IN

School name: University of Toronto

Vehicle name: Vortex

Vehicle number 5

Vehicle type Unrestricted ☑ Speed _____

Vehicle configuration

Upright ☐ Semi-recumbent ☑

Prone ☐ Other (specify) _____

Frame material: Carbon-fiber composite & structural foam

Fairing material(s): Carbon-fiber composite

Number of wheels: 2

Vehicle Dimensions *(please use inches, pounds)*

Length: 94.2 Width: 19.6

Height: 40.4 Wheelbase: 45.1

Weight Distribution Front: 19.6 Rear: 13.1 Total: 32.7

Wheel Size Front: ISO406 Rear: ISO406

Frontal area: 503.8 sq.in.

Steering Front ☑ Rear ☐

Braking Front ☐ Rear ☐ Both ☑

Estimated Cd: 0.071

Vehicle history (e.g., has it competed before? where? when?)

Vehicle has not competed previously, and is a new construction for the 2011 competition.

VORTEX

Unlimited-Class Human-Powered Vehicle

University of Toronto
Human-Powered Vehicle Design Team

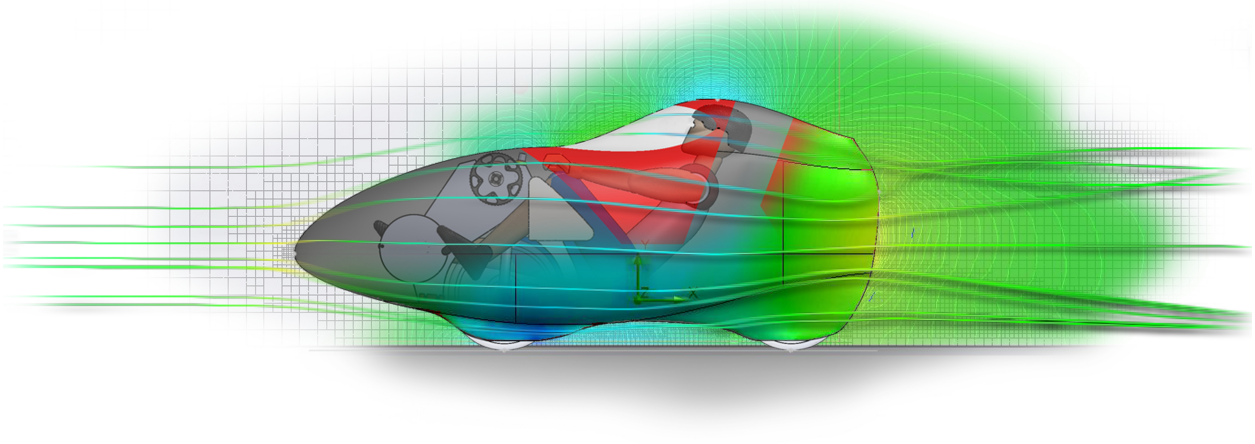

ASME Human-Powered Vehicle Challenge
Indianapolis Motor Speedway

April 29 - May 1, 2011

Contents

Abstract

The University of Toronto Human-Powered Vehicle Design Team will be submitting the $Vortex$ as an entry to compete in the Unlimited Class of this year's ASME HPV Challenge. The team's goal is to design, build and test a high-performance race vehicle that is also functional as a form of transportation. Specifically, the team has laid out three highly ambitious quantitative goals: to improve each of the weight, aerodynamic drag and handling quality rating by a factor of 2 over last year's highly-successful entry.

The configuration of choice is a front-wheel drive, monocoque-shell, similar to that of the previous year. However, a variety of innovative design features make the new $Vortex$ a vastly different vehicle. These include a body designed for 50% laminar flow with a simple and robust entry/exit method, a 3-point removable drive train for ease of maintenance and increased stiffness, an aerodynamically sealed cabin, a modular cargo system, a retractable landing gear, a roll-cage that is fully integrated into the aerodynamic shell, as well as lights, aerodynamic mirrors and a multitude of features for increased utility.

In depth analysis was performed on the handling of the vehicle as well as the aerodynamic design and the structural design of the monocoque shell. Testing was performed to determine rider configuration, material properties of various carbon fibre samples, the drag reduction obtained using several new aerodynamic features, and the best configuration for the landing gear. Construction of the vehicle is well under way, with the monocoque shell nearly complete and ready for final assembly. The combination of analysis and testing demonstrates a high probability that the team will achieve its stated objective of half the weight, half the drag, twice the handling, and infinitely more utility.

1 Innovation and Design

1.1 Design Objective and Product Specifications

Design Objective

Vortex is designed as a modular system that can be configured for both high-performance racing and as a practical form of transportation. It's race circuit includes top-speed, endurance and utility events at the ASME HPV Challenge, Human-Powered Race America series and the Human-Powered Speed Challenge at Battle Mountain. Its practical transport applications include urban commuting and longer-distance inter-city travel. Given the described scope, the team's 2011 mission statement is:

To design, construct and test a high-performance human-powered race vehicle that, when appropriately modified, can also be used for practical transportation. As an improvement over the 2010 ACE, the specific design objectives are to achieve half the weight ($M < 17kg$), half the aerodynamic drag ($C_D A < 0.027$), and half the Cooper-Harper Handling Qualities Rating ($HQR < 3$), while adding a variety of functional utility features. Due to the wide range of applications, the team's primary focus will be on innovative design solutions that

do not compromise the vehicle's race performance, safety or utility.

Design criteria and product design specifications

Success of the design will be evaluated based on three quantitative criteria: weight, which is easily measured; aerodynamic drag, measured using deceleration testing described in section 3.5; and handling qualities, measured using the NASA-developed Cooper-Harper Handling Qualities Rating [7]. Additionally, success will be measured by its ability to meet utility and safety goals, encapsulated in the design constraints below, and evaluated on a pass-fail basis.

Solo Operation	Easy ingress and egress
	Free-standing when parked, starting and stopping
Safety	Rollover and side protection (top load $> 600\ lbs$, side load $> 300\ lbs$)
	4-point safety harness
	Safe internal environment
	Rider skid protection
Manoeuvrability	Turn radius $< 25\ ft$
	Brake from 15 to 0 mph in $< 20\ ft$
	Two independent braking systems
Visibility	180° field of view
	Adequate front view
	Mirrors for adequate rear view
Utility	Storage for 1 gallon container and 15"h × 13"w × 8"d grocery bag
	Head/tail light, bell or horn, front/rear/side reflectors
	Mudguards or spray protection
	Theft protection
Power Delivery	Uninhibited pedal stroke

1.2 Evaluation of the current state of the art

Extensive background research was performed on the current state of the art in the four categories that correspond to team's primary design goals. In each category the top bikes were sought out, as in most cases, direct contact was made with the designers in order to gain greater insight into specific design and construction details.

Most aerodynamic: Currently the fastest bike in the world, the Varna Diablo boasts superb aerodynamics, primarily through smooth flowing curves and an extremely tight fit to the rider, made possible by meticulous placement and customization of internal components[6, 21]. Even more advanced aerodynamic concepts are found in Matt Weaver's series of speedbikes, including an accoustically-damped 70% laminar flow fairing and pressure-sealed cabin[20].

Lightest: The lightest production bike frame, the Cervélo R5ca (675 g), achieves it's required strength from directionally-optimized carbon layup[1]. The Amanita Virosa is the lightest fully faired recumbent at 11.5 kg, achieved through meticulous attention to weight at every step, a variety of custom carbon-fibre parts and a monocoque carbon shell[14, 17].

Best handling qualities: Both the Raptobike [10] and the M5 city racer [11] have been described

as good beginner recumbents. Built to maneuver in a city environement, they achieve their handling qualities through effective choice of centre-of-gravity location, head-tube angle, wheelbase and trail.

Most functional: One of the best selling velomobiles is the Quest, with ample cargo space, easy entry and exit and full-body suspension[9]. The configuration is designed to simplify common tasks such as loading, backing up and free-standing.

1.3 Evaluation of design alternatives

General Configuration

Last year an extensive study was conducted on the benefits of various configurations, including front-wheel vs. rear-wheel drive, front-wheel vs. rear-wheel steering and tubular frame vs. integrated monocoque structure. It was concluded that a front-wheel drive, monocoque structure resulted in the lightest, most durable and most efficient design. This year the team decided to keep with the same general configuration knowing that there is still room for extensive design innovations and improvements.

Design Choices

Table 1 shows the decision matrix for the primary components of the bike and subsystems designed to meet the vehicle constraints. Alternative solutions are evaluated based on the design criteria outlined in Section 1.1, that is weight, drag, handling and functionality, with their associated weights given in bold. Manufacturability is also listed, although the weighting is quite low since the team has decided to do whatever is required to make the best bike possible. Functionality in the table refers to how the solution addresses its particular constraint. Note also, that anything that allows the bike to be made smaller will improve the score for aerodynamic drag. The table clearly shows that many innovative solutions have come together to make *Vortex* significantly different, and significantly better than the 2010 *ACE*.

All of the major design solutions are discussed in greater detail in following sections. For simpler design choices, three general design principles guide the selection of components: first, available components are thoroughly researched and selected to minimize weight. Second, any utility-based solution that compromises weight or drag will be made removable, including wheel fairings, mirrors and lights. Third, no design solution is allowed to interfere with power delivery from the rider by impinging on the motion of the legs or putting the rider in a non-optimal position.

Quantified impact of weight and drag

It is important to be able to quantify the effect of additional weight or drag on race results, such as trap speed or lap time. To determine this, a computational race simulation was performed using the predicted weight, drag and rolling resistance of the vehicle, and using measured power profiles

	Ingress and Egress			Free Standing		Rollover Protection		Front Wheel Fairing				Mirrors			Storage			Spray protection		Regenerative Braking		Gear placement			Wheel design	
	Removable top shell	Square door cutout	Trip-line door cutout	Trike configuration	Landing gear	Internal	Integrated	Taco fairing	Envelope fairing	Flexible fairing	Rotating fairing	Standard arm mirror	Half-cone mirror	Integrated canopy bubble	External paniers	Extended rear section	Smaller rear wheel	Fenders	Inclosed wheel well	Electric	None	Hub	Mid-drive	Mid-drive centred	Standard	Thin custom disk
Weight **(5)**	3	4	4	2	4	3	4	4	3	3	3	4	3	3	3	3	5	4	3	2	5	5	5	5	4	3
Drag **(5)**	3	3	5	1	4	4	5	2	3	4	5	1	2	4	1	3	4	2	5	5	5	3	3	4	3	4
Handling **(3)**	5	5	5	5	4	5	5	5	5	5	5	5	5	5	4	5	5	5	5	5	5	5	5	5	3	4
Functionality **(5)**	1	4	4	4	3	5	5	1	1	1	1	4	4	4	5	4	4	3	4	4	1	2	4	4	3	5
Manufacturing **(2)**	4	4	4	3	4	4	4	5	4	3	4	5	3	3	4	4	4	4	3	1	5	5	4	2	5	2
Total **(100)**	58	78	88	56	75	83	93	60	58	61	68	70	66	76	65	73	88	68	81	72	80	75	83	84	69	76
2010 *ACE*	X					X		X				X										X			X	
2011 *Vortex*			X		X		X				X			X			X		X		X			X		X

Table 1: Design table

from one of the pilots. The table below shows the sensitivity of the race result to weight and drag with an example 10 kg mass increase and a 0.005 increase in C_dA. It also shows the break-even point, $(dx/dm)/(dx/dC_DA)$, which represents how much drag a given aerodynamic device must save per kilogram in order for it to be worth its weight. These results will be used to determine whether certain aerodynamic devices are worth their weight for a given type of race. It will also be useful in determining how much effort, time or money should be put into weight savings and drag reduction of specific components. It is interesting to note that the weight vs. drag break-even point is almost identical for the utility race and the $600m$ sprint event, due to the dominance of acceleration forces.

	Base	ΔM $10kg$	ΔC_DA 0.005	$\frac{dx}{dM}$	$\frac{dx}{dC_DA}$	$\frac{dx/dM}{dx/dC_DA}$
Endurance lap time (s)	93.2	95.8	94.6	0.26	280	0.00093
Utility lap time (s)	125.0	129.3	126.2	0.43	240	0.00179
$600m$ sprint speed (kph)	69.19	67.46	68.68	-0.173	-102	0.00169
Battle Mountain speed (kph)	123.46	122.67	119.66	-0.079	-760	0.00010

1.4 Innovation

Several design solutions deserve special attention as they represent an innovative feature that has not been employed on previous known vehicles.

Laminar flow body with easy ingress and egress

Extensive aerodynamic design was performed in order to achieve an extended laminar run over roughly 45% of the surface, which has the potential to reduce skin friction drag by 35%. The image below shows the current status of the completed shell, where the door lines have been cut just aft of the natural laminar trip point. This provides an easy entry method, without compromising laminar flow. Several previous vehicles have been designed for extensive laminar flow, but they were specifically made for World speed records and required a team to help the pilot in and out [20].

3-point removable drive train

The third attachment point on the drive train, shown in Figure 15, provides a substantial increase in stiffness, which helps with power delivery during sprints and helps eliminate chain rubbing and derailment which had caused chain derailment issues in the past. Additionally, the entire drive-train assembly is removable with three quick-release skewers, so it can be set on a separate stand for easy maintenance. Finally, the drive assembly boasts a centered mid-drive that reduces the width of the assembly allow for a smaller Q-factor and a tighter aerodynamic shell.

Integrated canopy bubble mirrors

Figure 15 shows the placement of the canopy mirrors, which are close to the eyes for the greatest field-of-view. They are aerodynamically integrated into the canopy bubble to minimize drag losses, which would otherwise be quite severe for a mirror with a flat back.

Integrated rollover and side protection system

The rollover and side protection system has been designed such that it adds virtually zero additional space within the shell. The image below shows how the rollover structure is an integral part of the aerodynamic surface, and with its position aft of the laminar trip point, it's impingement on aerodynamics is effectively eliminated.

Figure 1: Current status of construction, with monocoque shell complete.

2 Analysis

2.1 Vehicle Handling

Objective: To determine the steering geometry of the bike such that it is stable and is easily controllable at the speed range of 0 to 140 kph. Specifically, the goal is to achieve a significant increase over the 2010 ACE with a Cooper-Harper Handling Quality Rating of 3 or less.

Analysis Case Definitions: The design variables for the steering configuration are the head angle and wheelbase. An off-the-shelf fork was modified to accept ISO406 size wheels instead of the normal 700c, and as such the offset of the wheel axis relative to the steering axis is fixed at 24.8 mm.

Modelling: Two software tools have been used in determining the stability and control of the bike. The "hands-off" stability of the bike was analyzed with JBike6, a software package uses the linearized equations of motion of a bike system around the upward equilibrium position. The outputs of the software are the weave and capsize velocities. The second tool used is a custom Matlab code written using the equations outlined in Lords of the Chainring [15]. This code calculates the perceived response of the bike to a rider and uses four parameters to indicate the controllability of the bike. Each of the parameters has an upper and lower bounds, outside which the behaviour of the bike is undesirable, described below and marked with vertical lines in Figure 2b.

Parameter	*Interpretation*	*Acceptable range*	*Issues below range*	*Issues above range*
Wheel Flop F (Nm/rad)	Feeling of COM moving down when steering	50-300 Nm/rad	Little feel for lean, steering angles	Instability once turn has started. Dangerous at high speeds.
Control Authority K	How much control the user has over the roll angle	> 3, higher if low speed control is important	Rider must initiate large turns to keep bike vertical	Unspecified
Steering Stiffness K_1 (Nm/rad)	How much stiffness the rider perceives to be in the handlebars	0-25 Nm/rad	Instability, as negative stiffness implies the machine will veer out of control	Too much control force needed, oscillation period become too short to handle
Steering Sensitivity S $(rad/s \cdot m)$	How much the roll angle changes for a given steering displacement	5-18 $rad/s \cdot m$	Bike is sluggish, needs large steering inputs to change roll angle	Bike is too sensitive, any small input changes roll angle

Results: A sweep of steering angles between 75° and 90° was performed, and the results from JBike6 and the custom Matlab code are shown below. Figure 2a shows the weave and the capsize speeds for head tubes angles 70° to 90° degrees as well as the capsize and weave velocities of the 2010 ACE and a Schwin cruiser bike. The bike is self-stable between these two critical speeds, implying that the bike will have better low and high speed stability as the head angle approaches 90°.

Figure 2 shows the behaviour of the four controllability parameters for the range of head angles. The Control Authority is above the minimum value of 3 and doesnt change much for the angles considered. The wheel flop is unacceptably high at low angles but becomes reasonable near 80°.

Above 80° head-angle sensitivity becomes unacceptably high ($> 23 rad/s \cdot m$) the steering stiffness becomes dangerously low ($< 5 Nm/rad$). 80° was therefore chosen as the best compromise. The wheelbase was found to have a small effect on controllability, but a big effect on aerodynamic efficiency, since a shorter wheelbase allows for a small bike. It was therefore decided to shorten the wheelbase compared with the 2010 ACE to $1.145m$.

Given that the addition of a steering damper on the ACE, described in Section 3.6, was able to improve the Cooper-Harper Handling Quality Rating from 6 to 3, and given that Figure 2 shows an improvement in stability and controllability over the ACE, the team is confident that the $Vortex$ will meet the design criteria of having an HQR < 3.

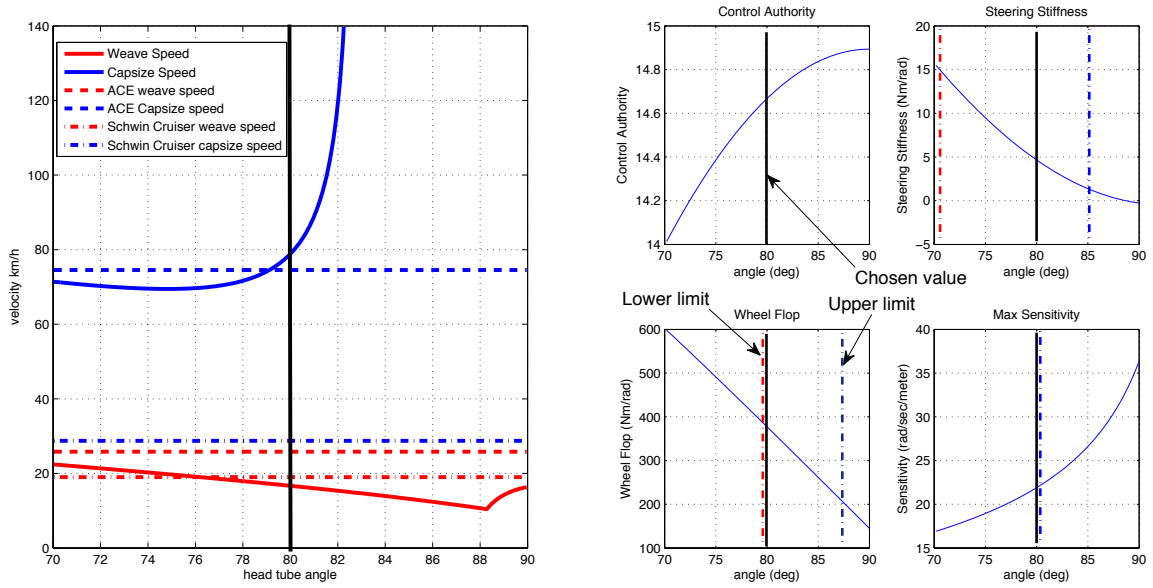

(a) (b)

Figure 2: (a) Stability and (b) Controllability results.

2.2 Aerodynamic Design

Objective: Minimize aerodynamic drag, subject to the rider constraints outlined in Section 3.3. Specifically, the goal is to reduce the drag to half of it's 2010 value, namely $C_D A = 0.027$.

Analysis Case Definitions: There are three main aspects of the aerodynamic design, outlined below. The first will be implemented without detailed analysis, while the second two require extensive design described in detail in the pages that follow.

1. Inclusion of empirically-based aerodynamic strategies and devices: The following devices will be integrated into the design based on research, discussion with experts in the field [4, 19, 20, 3, 8], and drag data described in Section 3.5. Wheel wells will fully enclose the

wheels to reduce centrifugal pump losses; wheel fairings with an appropriate leading-edge fillet will eliminate horse-shoe separation; filleted corners will reduce junction drag; smooth changes in curvature will reduce flow overspeeds; a fully sealed cabin will reduce internal flows; ventilation entry at the high-pressure canopy region and exit at low-pressure trailing edge, with appropriate divergence and convergence nozzles, will minimize ventilation drag.

2. Design of a robust, laminar boundary layer: Given that laminar boundary layer has 90% less drag than a turbulent one [8, 19], pressure profiles on the front half of the vehicle will be designed to support an extended laminar run that is robust to cross-winds and road vibration.
3. Design of a minimum-drag pressure recovery curve: In the pressure recovery region, beyond the rider's shoulders, the curvature should be designed to allow for the shortest possible tail, while preventing flow separation.

Modelling: FlowWorks is a low-level CFD package that is fully integrated into SolidWorks, the team's choice of CAD software. It can be used to generate pressure profiles along the streamlines, but as a low-level package it is not accurate in resolving boundary-layer transition or flow separation. Knowing the pressure profile along various streamlines, however, XFOIL, a highly-accurate low-speed 2D flow solver, will be used to predict transition and adjust the pressure profiles appropriately. Separation on the aft portion of the vehicle will be predicted with the Stratford turbulent separation criteria, which states that separation will occur when $\bar{C_p}\left[x\left(d\bar{C_p}/dx\right)\right]^{1/2}\left(10^{-6}Re\right)^{-1/10} > 0.35$, where x is the distance along the chord, Re is the Reynolds number and $\bar{C_p} = \left(C_p - C_{p,min}\right)/\left(1 - C_{p,min}\right)$ is the canonical pressure coefficient [18]. The Stratford criteria is extremely useful in designing the pressure recovery because it determines exactly how close the flow is to separating at any given point. The ideal Stratford recovery curve is one where the flow is equally close to separating along the entire pressure recovery region, which leads to the shortest possible tail and the lowest theoretical drag.

Robust natural boundary layer design and results: Based on the aerodynamic strategies outlined above and an intuitive understanding of how the pressure profile affects boundary layer transition, a first iteration fairing shape was created. The pressure profile along the side of the vehicle was used to create an "equivalent" 2D airfoil in XFOIL, which could then be modified to produce a profile that extends the laminar run while being resistant to road vibrations and cross-winds. A value of $N_{crit} = 0.25$ was used in XFOIL to simulate bypass transition caused by road vibration or surface imperfections [5], and the Reynolds number was set to the highest conceivable value of $6x10^6$, in order to simulate the most challenging scenario for maintaining a laminar boundary layer.

A series of tests were performed to gain an understanding of how the pressure profile affects transition. Figure 3a shows the resulting drag vs. angle of attack with the baseline case given by `robust`. First, it was found that an increase in the leading-edge radius of the airfoil (`robustler`) led to pressure spikes that decreased the width of the "drag bucket", implying that transition is more susceptible to cross-winds. Next, modifying the curvature of the airfoil to produce a steeper pressure gradient (`robustslope`) was found to significantly extend the laminar run and drastically

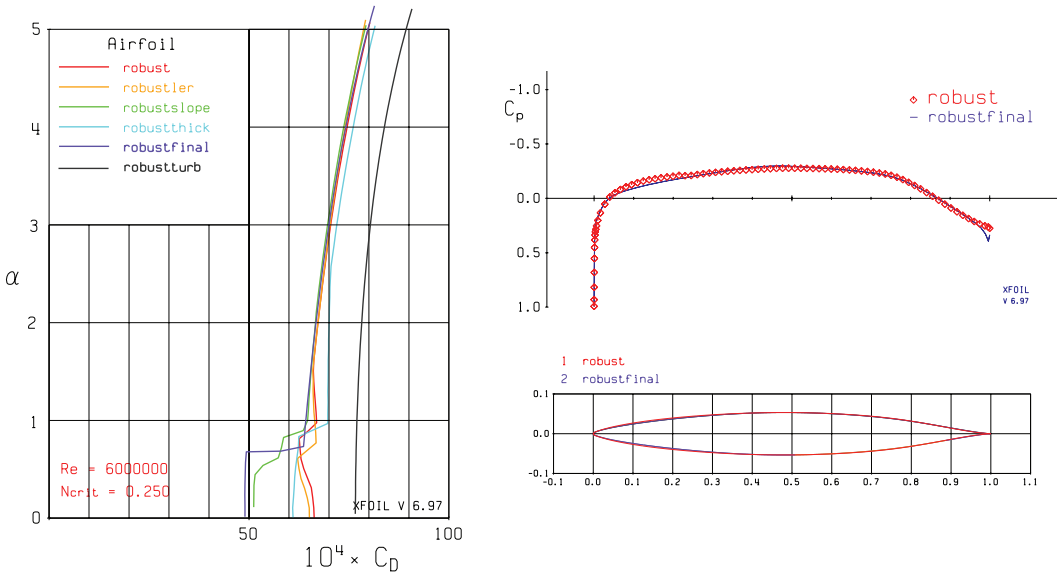

(a) (b)

Figure 3: (a) Drag polars of various test airfoils (b) Resulting pressure profile.

reduce drag. Finally, increasing the thickness (`robustthick`) was found to extend the laminar run since it inherently steepens the pressure gradient, but unfortunately it shifts the entire drag curve up because of higher overspeeds. These tests provided guidance for a series of iterations that led to the final shape (`robustfinal`), which employs a sharper leading edge and a steep constant slope in the pressure profile (Figure 3b) up until the point of transition at 48% of the chord. This results in a drag reduction of 35% over the fully turbulent case (`robustturb`), which holds constant until α reaches 0.65° and the transition location jumps to the leading edge. A 2D angle of attack of 0.65° corresponds to a cross-wind angle of roughly 6.5° for this particular vehicle [16], implying that at $60kph$ extensive laminar flow on both sides of the vehicle will be achieved if cross-wind gusts are under $7kph$.

This optimum 2D pressure profile was implemented in final vehicle design through successive changes to the shape and computational runs using SolidWorks FlowWorks. Figure 5 compares the pressure profiles along the side of the bike for several design iterations, as the slope is gradually improved. Figure 4 shows the streamlines and the resulting pressure profiles along those streamlines for the final vehicle design. The presence of the canopy bubble, front wheel fairing and the presence of the ground all impacted the 3D pressure profiles, but in the end, a steep, linear pressure gradient similar to the optimal 2D profile was achieved over the entire front surface.

Stratford pressure recovery design and results: The ideal Stratford pressure recovery profile has a steep initial slope that gradually decreases towards the tail. This implies a high initial curvature around the shoulders and a cusped trailing edge. Figure 5 shows the resulting pressure

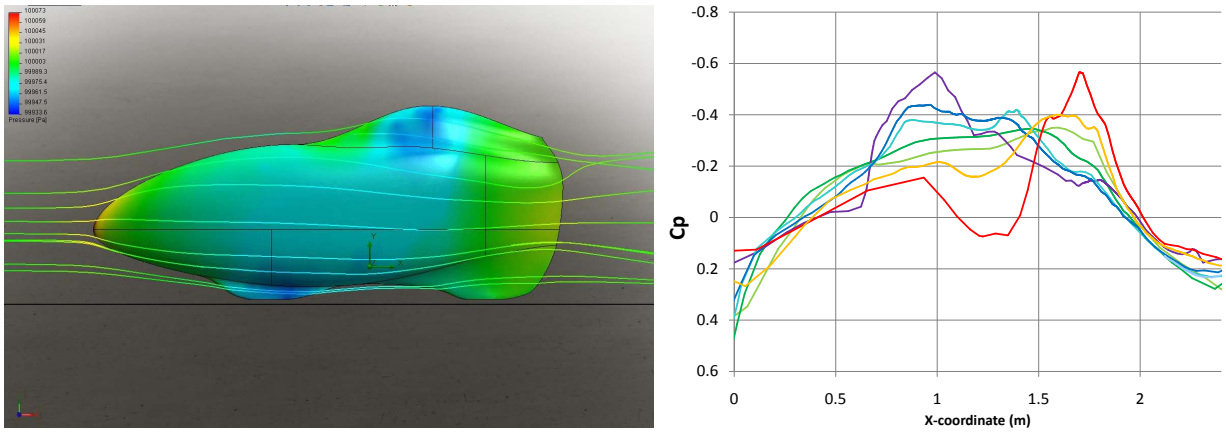

(a) (b)

Figure 4: (a) Streamlines and pressure map computed using FlowWorks and (b) resulting pressure profiles. The purple line is the lowest streamline, that passes by the front wheel fairing, and the red line is the highest streamline, that passes over the canopy.

profiles and Stratford coefficient, S, along the side of the bike for several design iterations. Small changes in curvature, and an increased trailing-edge cusp, eventually led to a small value of S over the entire recovery region. Since separation is highly dependent on speed, the plot shows S at the "separation speed" of 43 kph, when S is equal to the critical value of 0.35. Above this speed S will be lower and the flow will be entirely attached, whereas below this speed, when aerodynamics are not as critical, small areas of separation will be present behind the shoulders.

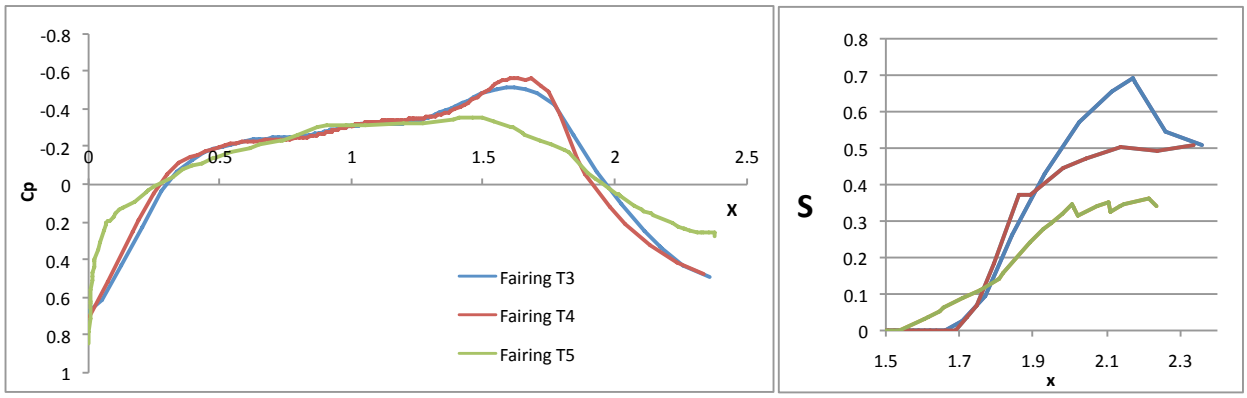

(a) (b)

Figure 5: Pressure coefficient (a) and Stratford coefficient (b)for several design iterations.

Final drag predictions: When compared with the 2010 *ACE* the surface area has been reduced by 45%, the extent of laminar flow has been increased by nearly 40%, and drastic improve-

ments have been made to the fairing and sealing of the front wheel. Using a semi-empirical model developed from equations outlined in [19] and drag data collected for various aerodynamic devices such as wheel wells and wheel fairings (described in detail in last year's report[13]), the final drag area is estimated to be $C_DA = 0.023$. This represents a substantial reduction of over 50% from the 2010 *ACE* ($C_DA = 0.054$), meeting the ambitious design criteria set out at the beginning of the year.

2.3 Structural Design

Objectives: The objective of the structural analysis is to obtain the lightest structure possible, while still satisfying the critical design load cases for stiffness and strength. Specifically the goal is to obtain a final vehicle weight under 17 kg.

Analysis Case Definitions: The composite structure is comprised of a woven carbon fiber (CF) shell, and 9 unidirectional CF and Divinycell-F sandwich primary structure members as shown in Figure 6. The *front-ring* and *middle-semi-ring* provide three attachment points for the drivetrain structure; 2 *gunwales* bridge the front and rear structures (for occupant-imposed loads); the *rollcage* serves as the RPS; and the *rear-axle stays* and *rear-axle beams* carry the rear wheel loads to the rollcage.

The rollover and side protection system (RPS) is designed to protect the occupant from both inertial loads and crush loads. The worst-case loading between these two scenarios was chosen for each RPS case. Two other critical load cases are defined below.

RPS Top Load: In the 600 lb crush-load case, the bottom extremity of the rollcage was immobilized (also near the rider CG, simulating the inertial load case), and the crush/impact force was applied on the top arch. The forces were applied as distributed loads in order to better simulate the proof-loading test for validation, but the location and magnitude of the maximum stress was almost identical with a point load.

RPS Side Load: The worst-case side-load scenario was the inertial load case, in which the RPS is fixed at the bottom surface (as in the top load case, near the rider CG), and the 300 lb force is applied horizontally at head-level (as would be imposed by a side-impact). This loads the rollcage in a cantilever-like manner, resulting in higher stresses than a side-to-side crush analysis.

Rider Gravity Load: In this case the rider CG is fixed (again, assumed to be the bottom surface of the RPS) and a 1 kN upwards load is applied on each of the drivetrain structure (where the headtube is bonded) and the rear axle. This 2 kN load is meant to represent a maximum weight rider (250 lbs) with $2g$ factor (the 2010 vehicle was tested in a velodrome where g-loading approached this level). *Maximum Pedal Push:* In this case the maximum force a rider could apply was considered. The vehicle was constrained at the RPS shear wall (where a rider's back would push) and the force was applied forward at the bottom bracket. A total force of 2 kN was chosen, as the maximum any rider on the team could leg press (with both legs) was 1000 lbs.

Modelling: Stress analysis using 3-node membrane finite elements was conducted using Solidworks Simulation. A surface-based model of the woven CF shell and sandwich primary structure was

generated, located as determined by the human model, wheel hardpoints, and drivetrain attachment locations. A surface model allows for the most accurate composite laminate definition in Simulation. The laminate properties were anisotropic, with the 0-direction (i.e. primary fiber direction) being aligned with a) long-axis of the vehicle for the woven laminate, b) along the circumferential direction of each of the three-hoop/semi-hoop structural reinforcements, and c) along the primary load direction for the gunwale and rear axle truss. The material properties assigned were determined from material testing data described in Section 3.2 and manufacturer testing properties. Fixed-displacement constraints were applied to appropriate surface patches for each analysis, indicated by green arrows in the resulting figures. Forces were applied as distributed loads on the appropriate surfaces, indicated by purple arrows.

Design Modifications: The design was modified iteratively using the stress analysis (results provided are with final structural design). The thicknesses of structural laminates were modified in discrete plies: the woven material was a $5.0 oz/yd^2$ plain-style CF with ply-thickness of $.15mm$, and the unidirectional material was a $4.7 oz/yd^2$ uni-tape with ply-thickness of $.3mm$. The sandwich-core thickness was fixed at $.5in$, for maximum specific performance without intruding on the occupant envelope in key areas. The baseline thickness for each member was based on the 2010 vehicle, and optimized as follows. The woven shell laminate was initially reduced by 50% (to 2 plies), to provide only aerodynamic fairing and structural stabilization. This resulted in FOSs being less than 2 in some cases, whereas a shell thickness of 3 plies was sufficient. For primary structural members, the laminate thickness was adjusted to optimize the worst-case FOS (3 in general for manufacturing variability, but 5 for the RPS for maximum safety). A special case was the rider gravity load case, which has a high FOS for the static load, but provides margin for the wheel shock encountered in everyday riding. The drivetrain structure, floorboard, and RPS shear-wall were each fabricated from aircraft sandwich panel (.4" honeycomb core with .014" woven CF faces) for ease of manufacture. The shear wall is one panel thick (determined by load testing in 2010) and the drivetrain structure varying between 2 and 4 layers as required for stiffness of the transmission (to prevent chain-derailment). The floorboard is two panels thick to accommodate drivetrain mounting hardware. The final material thicknesses were as follows (per sandwich face): the front ring, gunwale, rear axle triangle-stay, and rear axle triangle-beam were all 3 plies, the RPS rollcage was 4 plies, and the middle semi-ring was 2 plies.

Results: The stress field results were mapped as the worst-case von Mises stress across all plies of the laminate. In each load case, the unidirectional sandwich primary structure and shell structure were viewed for worst-case stress independently to ease identification of the highest-stress and calculation of the Factor-of-Safety. See table 2 for results of finite-element analysis on the composite shell and primary structure, with both stresses and FOSs compiled. Also, see figures 6, 7, 8, and 9 for primary structure and shell stress-maps for the RPS top load & side load, rider gravity load, and max drive push cases respectively. The primary structure described above has recently been completed at a total weight of 9.8 kg. The estimate for the remainder of the components based on last year's vehicle is 5 kg. This puts the total predicted weight at 14.8 kg, well below half the

weight of the 2010 *ACE* (34 *kg*) and easily meeting the stated design objectives.

Analysis Case	Struct. σ_{max} [Pa]	Struct. FOS	Shell σ_{max} [Pa]	Shell FOS
RPS Top Load (600 *lb*)	366.9E6	5.15	172.5E6	2.85
RPS Side Load (300 *lb*)	282.0E6	6.70	113.1E6	4.35
Rider 2G Load (2 *kN*)	63.1E6	29.9	74.6E6	6.59
Max Pedal Push (2 *kN*)	250.8E6	7.53	58.1E6	8.47

Table 2: Results of Solidworks composite analysis for four design load cases.

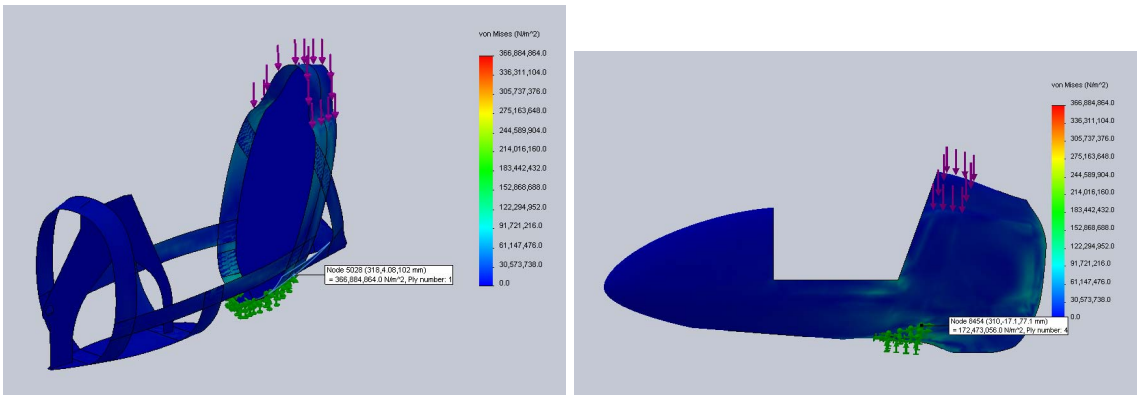

Figure 6: Results of RPS top load analysis, with primary structure and shell isolated.

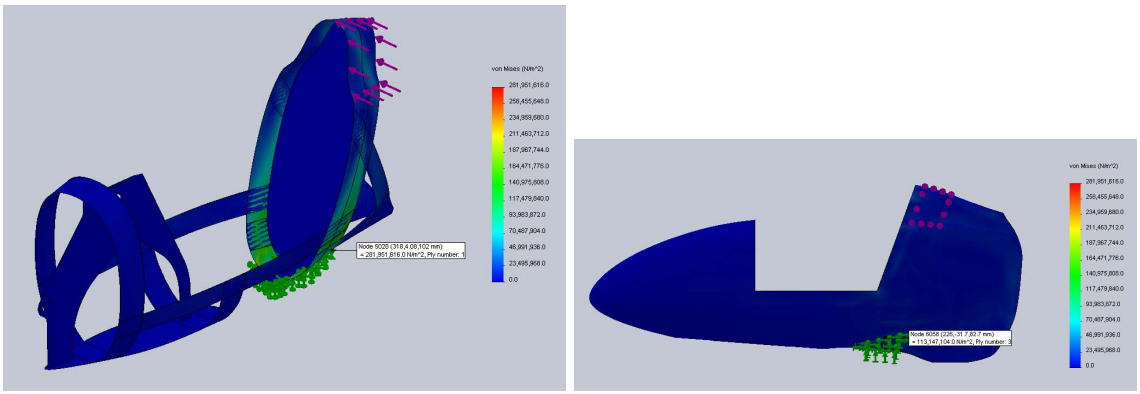

Figure 7: Results of RPS side load analysis, with primary structure and shell isolated.

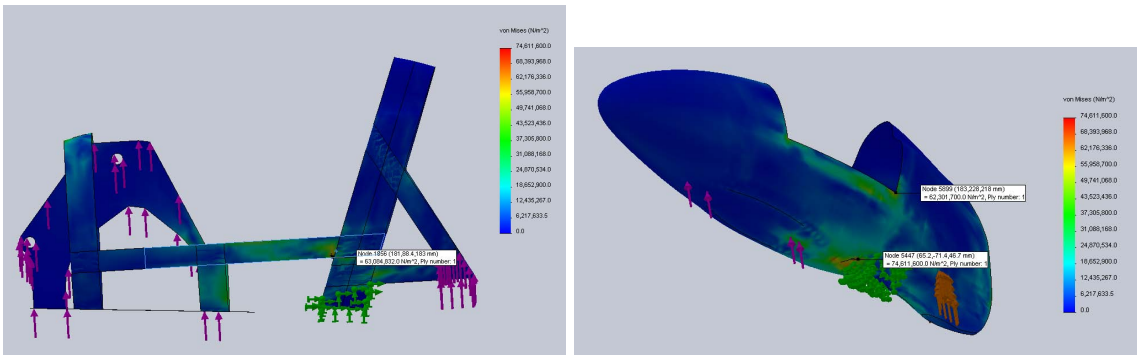

Figure 8: Results of rider gravity load analysis, with primary structure and shell isolated.

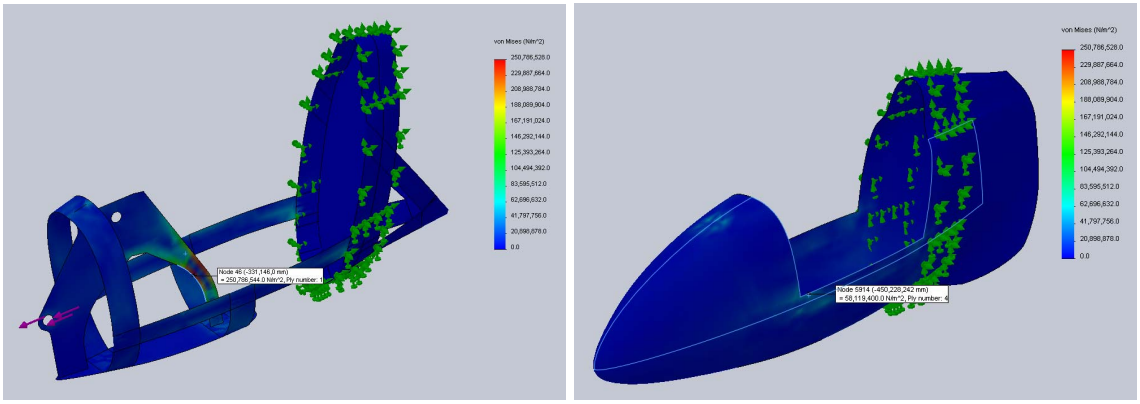

Figure 9: Results of maximum pedal push analysis, with primary structure and shell isolated.

2.4 Cost Analysis

The total production cost of the *Vortex* for this year's competition is $8,075. The Net Present Value method was used to calculate the 6 years production cost at a 2% interest rate. A production run of 6 years at a rate of 10 vehicles per month would cost $15,069,002 in today's currency. An initial investment of $6,840 is required for various machines and tools. The mold construction cost is $3,495 per mold. The vehicle materials cost per vehicle is $4,211. The labor cost per vehicle is $74,490 including design cost and component machining and assembly costs. The overhead costs of the production facility is $3,500 per month. A detailed breakdown of the costs can be found in the table below.

Cashflow period	0 Year 1	1 Year 2	2 Year 3	3 Year 4	4 Year 5	5 Year 6
Equipment Capital	$6,840					
Tooling	$2,000	$2,000	$2,000	$2,000	$2,000	$2,000
Vehicle Materials	$505,320	$505,320	$505,320	$505,320	$505,320	$505,320
Mold Construction	$3,495	$3,495	$3,495	$3,495	$3,495	$3,495
Labour Costs	$2,129,850	$2,073,600	$2,073,600	$2,073,600	$2,073,600	$2,073,600
Overhead Costs	$42,000	$42,000	$42,000	$42,000	$42,000	$42,000
Total Costs	$2,689,505	$2,626,415	$2,626,415	$2,626,415	$2,626,415	$2,626,415
Present Value	$2,689,505	$2,574,917	$2,524,428	$2,474,930	$2,426,401	$2,378,825
Net Present Value	$15,069,006					

Vehicle Materials (per vehicle)	
Components (off-the-shelf)	$1,385
Metal Stock for Components	$240
Composite Materials	$2,460
Vacuum Bagging Consumables	$126
	$4,211

Mold Construction (per mold)	
Fairing Plug Manufacture	$2,150
Mold Cavity Manufacture	$1,345
	$3,495

Overhead Costs (per month)	
Factory Rental	$2,500
Utilities	$1,000
	$3,500

Labor Costs (per vehicle)	
Development Cost (750hr @ $75/hr)	$56,250
Machining Cost (16hr @ $60/hr)	$960
Assembly Cost (288hr @$60/hr)	$17,280
	$74,490

Machine and Equipment Capital	
Vacuum Pump	$2,300
Fittings and Hose System for Pump	$240
Hand Tools	$100
Power Tools	$100
Milling Machine	$4,000
Drill press	$100
	$6,840

3 Testing

3.1 Rollover and side protection system

Objective: The objective of the RPS testing is to validate the stress analysis performed during the design phase, ensure manufacturing standards, and ensure occupant safety.
Methodology (Top Load): The top load test is designed to mimic the impact loads of a top-to-bottom crush on the rollcage structure. A gravity load will be applied using calibrated masses. The integrated RPS and shell are supported on the lower exterior surface of the rollcage. The support is fabricated from wood to hold the RPS in the vertical plane, with high-strength polystyrene adjacent to the shell surface to evenly distribute the reaction force. The rollcage top surface load distribution is replicated using a wood frame and polystyrene surface contact pad. Loads are applied in 100 lb increments, up to a total load of 600 lb. During load application, the structure is closely monitored for audible (e.g. crackling, strain relieving) and visible (e.g. sudden displacement, cracks) signs of imminent failure, with displacement measurements taken at each increment.
Methodology (Side Load): The integrated RPS is fixtured in the same support for the side load test as for the top load test, with the rollcage clamped to one side to resist the moment applied by the side load. Force is applied with calibrated weights under gravity load, rotated to a side force using a pulley. The load is applied in 50 lb increments, while the structure is monitored for signs of failure, with displacement measurements taken at each load increment.
Results and Conclusions: As proof-loading the competition vehicle and validating its manufacture will be the best option for ensuring rider safety, this test cannot be completed until the full shell is assembled. As such the results will be presented in the 2 page update prior to the competition.

3.2 Composite Materials Properties Testing

Objective: To determine critical material properties for the woven and unidirectional composites used in the modelling and design of the vehicle, namely the Young's Modulus and Ultimate Strength in the fiber directions.
Methodology (Woven Laminates): Four vacuum-bagged flat-panel test specimens of woven 0/90 carbon-fiber epoxy laminate were tested at UTIAS in the materials testing laboratory. The articles were dogbone-style, with a neck 10mm wide by 0.5mm thick, and aluminum gripping tabs bonded to the ends (Figure 10). Loads were applied via a 100 kN MTS hydraulic load frame, under constant displacement control. Strains were measured in three ways: strain gauges adhered to the dogbone neck, laser-extensometer measurements between reflective tapes, and speckle interferometry using random spray patterns applied to the specimen surface.
Methodology (Unidirectional Laminates): Unidirectional laminates were tested using a 3-point sandwich beam setup (Figure 10) primarily because unidirectional laminates are difficult to machine into dogbone specimens and a premature failure in the matrix along the fiber direction is often encountered in tensile testing. Testing was done with a static-load rig and precision masses

were used. Twelve sandwich beam specimens were manufactured, with a width of 25 mm and depth between 6.35 mm and 12.7 mm.

Results and Conclusions: Table 3 shows the results of the unidirectional and woven laminate testing, as well as comparison figures from industry. Due to premature grip failure, statistical analysis was not available on the woven failure tests. The team's woven laminate test figures are likely lower due to a) reduced fiber volume fraction, b) lack of elevated-temperature post cure of the specimens (recommended for optimal performance), and c) gripping issues (especially for failure data). The reduced unidirectional modulus is possibly due to measurement precision in the geometry of the sandwich structure. The reduced failure strength, similar to figures previously observed in this format of HPVDT testing, is possibly a result of premature failure due to indentation under 3-point load as well as face-sheet delamination that was sometimes observed (but which may have precipitated face failure).

Design Modifications: The data obtained was used in the FEA of the composite structure, as mentioned previously. Discrepancies noted in the material strengths were addressed with the use of a post-cure cycle for the composite vehicle structure.

Test Case	E [Pa]	$\sigma_E[Pa]$	Δ_E	σ_u [Pa]	σ_{σ_u} [Pa]	Δ_{σ_u}
Woven Laminate - Tested	51.4E9	6.4E9	-8.7%	492E6E6	N/A	-5.7%
Woven Laminate - PTM&W	56.3E9	-	-	521.5E6	-	-
Uni. Laminate - Tested	163.3E9	16.1E9	-3.9%	1,890E6	151.6E6	-21.3%
Uni. Laminate - Hexcel	170E9	-	-	2,400E6	-	-

Table 3: Results of unidirectional and woven composites testing, including standard deviation.

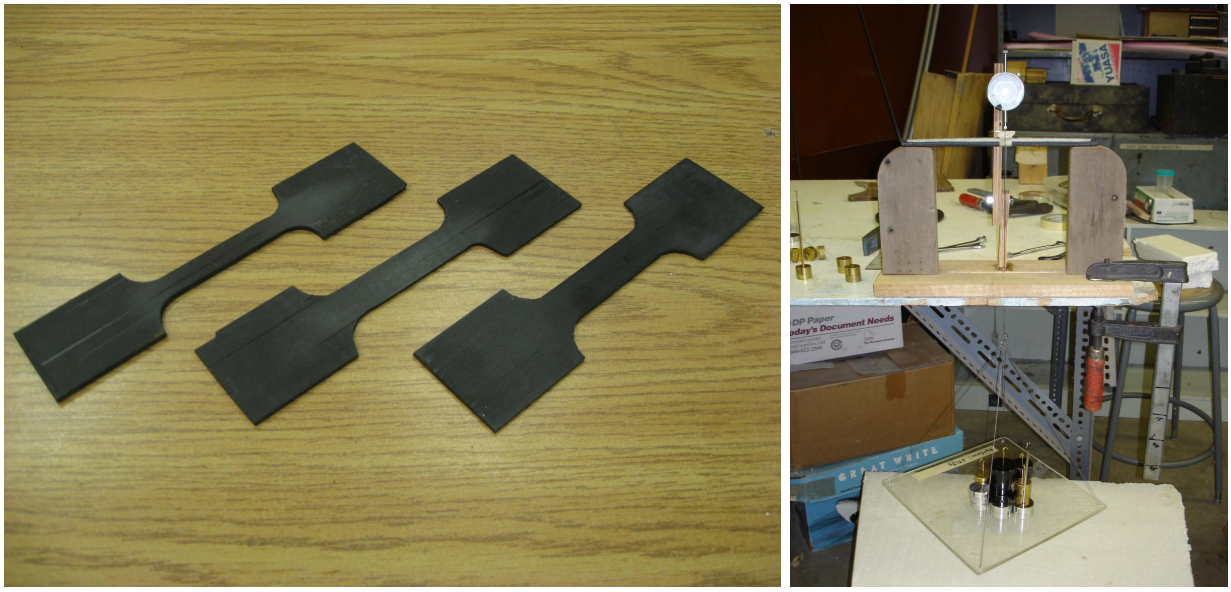

Figure 10: Dogbone woven test specimens and 3-point sandwich beam testing for unidirectional laminates.

3.3 Rider Configuration

Objective: To determine the optimal position for the rider, considering aerodynamic, structural and performance constraints.
Methodology: The pilot position in a streamlined vehicle is of paramount importance in determining attainable performance. The aerodynamic shape must be designed to allow the pilot to pedal in an efficient and safe manner and also have a good view of the surroundings. A wide range of riders need to be able to fit in the bike, as the shortest team member is 5.2 ft and the tallest 6.3 ft. To allow for a quick driver change and simple structure, the pedal position as well as the handlebar position are not changed; instead, the seat of the rider is custom molded for optimal fit. To ensure a tight fairing fit around the rider, a jig system was constructed to allow each riders pedal stroke to be measured, as seen in Figure 11a. The back and lower-back rests as well as the shoulder and hip vertical walls were adjustable. Main constrains were that the rider must be able to see over the handlebars and that the knees must clear the handlebars. Two parameters were varied, the overall back angle of the rider and the height of the bottom bracket above the plane of the seat.

		Seat Angle				
Comfort(1-10)/Power(1-10)		35°	40°	45°	50°	55°
Pedal Height	200mm	8/4	8/5	8/6	6/4	6/4
	220mm	7/4	7/5	8/7	7/5	6/4
	240mm	7/3	8/6	9/8	6/7	5/6
	260mm	6/4	6/5	7/7	5/6	4/7
	280mm	5/5	5/6	7/8	4/5	3/6

Results and Conclusions: The optimal seat angle and bottom bracket height were determined to be 42° and 240 mm respectively. With the rider position fixed, the jig was used to determine the minimum dimensions of the fairing such that it would not interfere with the rider. A solid-model rider constraint block was created showing the outer limits of the rider envelope, and was used in the aerodynamic design to determine the fairing shape (Figure 11b). The pedal area was paid close attention to and cross-sections were used to determine the precise pedal positions while the rider applied power.

3.4 Landing gear

Objective: To test several different landing gear configurations to determine the best design choice.
Methodology: Due to the need to start and stop without assistance, a landing gear needs to be designed to stabilize the bike at low speed. A number of landing gear examples were seen during the 2010 Michigan HPV rally, especially on the Baracuda and Moby 23 streamliners. Two landing gear configurations were considered: a sliding tube mechanism, similar to the one on the Baracuda

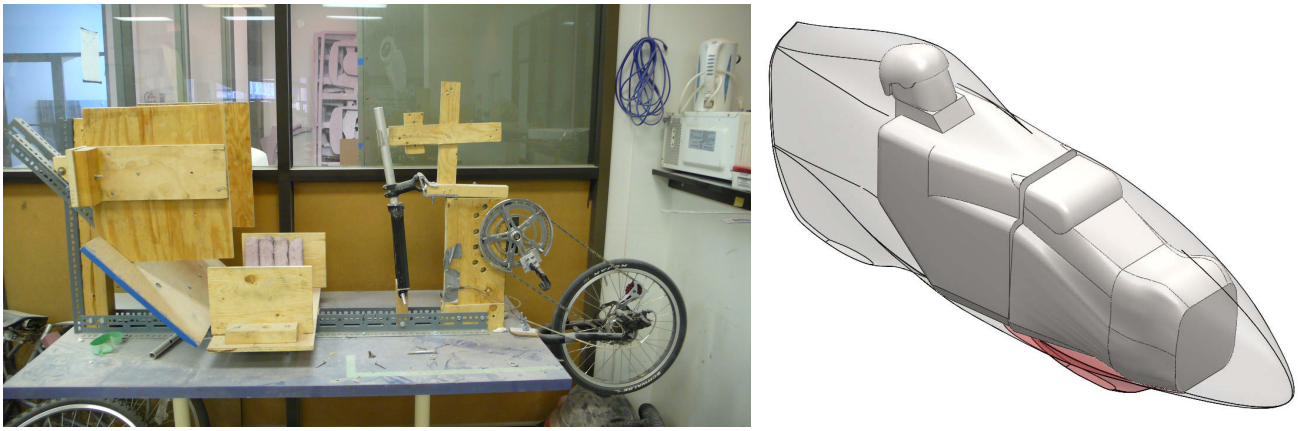

(a) (b)

Figure 11: (a) Test rig and (b) rider constraint block.

and Moby 23, as well as a pivoting arm configuration, similar to the landing gear on airplanes. A prototype of each was built and attached to a low-racer recumbent.

Results and Conclusions: The two mechanisms were rated on several factors and it was decided that the sliding tube was the preferred option. A view of the retracted and deployed landing gear on the new vehicle can be seen in Figure 12.

	Sliding tube	Pivoting arm
Weight (kg)	2	1.5
Robustness (1-10)	7	8
Reliability (1-10)	8	6
Ease of actuation (1-10)	10	6

3.5 Aerodynamic Testing

Objective: First, to determine a practical and accurate method for measuring the aerodynamic drag of the vehicle, and second, to obtain a quantitative measure of the effectiveness of several aerodynamic devices.

Methodology: Aerodynamic devices such as wheel fairings, sealed wheel wells, ventilation and disc-wheels involved complex internal and separated flows that are not easily computed with analytical or computational models. Wind-tunnel force data would be the most precise method for determining the specific impact of these devices: however, unless the wind tunnel has a moving floor with the wheels turning at the same velocity, the results would be highly inaccurate. As the next best option, measuring the zero-pedal-force deceleration of the vehicle can yield accurate drag measurements. Three locations were tested: the race strip at the World Human-Powered Speed Challenge in Battle Mountain, Nevada, the 2 km runway at Downsview Airport in Toronto, Ontario, and the indoor Forest City Velodrome in London, Ontario. The 2010 ACE was outfitted

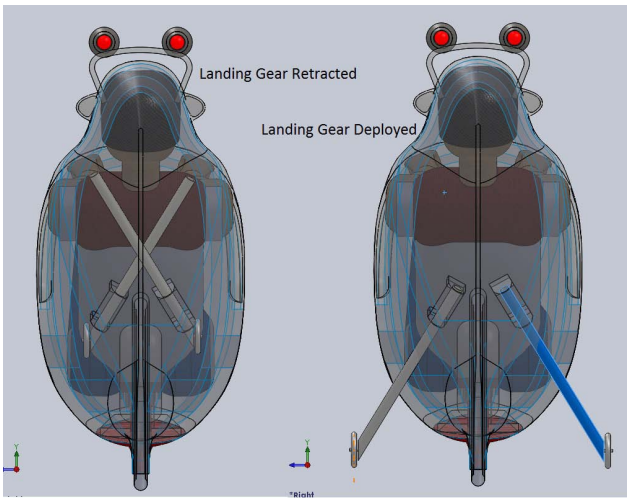

Figure 12: Final landing gear design.

with three new aerodynamic devices (not used at the 2010 ASME race): a front wheel fairing that fully enclosed the wheel, a rear wheel well that sealed of the rear wheel with approx. 2 cm of clearance, and discs that could be mounted on the wheels to simulate a disc-wheel. Measurements were taken with an onboard Eagletree Flight Data Recorder equipped with GPS speed, rpm-determined ground speed, wind speed, and temperature recording devices. Speeds were recorded as the vehicle decelerated from its top speed and the acceleration was plotted against velocity. Fitting the curve to the equation below results in an estimate for the drag area C_D [19].

$$\dot{U} = \frac{C_{rr_1} mg + C_{rr_2} mgU + 0.5\rho C_D A U^2}{m + I/r^2}$$

where U is the velocity, m the mass, I the wheel inertia, r the wheel radius, g the gravitational acceleration, A the frontal area, and C_{rr_1} and C_{rr_2} the rolling coefficients. For details of the coefficients and values used see [22].

Results and Conclusions: It was concluded that outdoor testing could not be sufficiently accurate due to wind forces, even if they were quite small. Even with wind speed measurement using a pitot tube and accurate ground slope data, measurement error was far too great. Indoor testing proved to be repeatable as long as all factors such as tire pressure, vehicle and rider weight, temperature and air density are accurately measured. The results from the indoor velodrome testing are shown in the table below:

Test	Mean	StDev	95% confidence interval	% Change	Data Points
Fully Aerodynamic	0.0980	0.00534	0.08952 - 0.10653	-	4
Fairing removed	0.1097	0.00333	0.1014 - 0.11794	+12.1 %	3
Fairing and wheel well removed	0.1121	0.00445	0.10104 - 0.12316	+2.2%	3
Fairing, wheel well and wheel disc removed	0.1077	0.00416	0.09737 - 0.11803	-4.1%	3

By helping to seal the front wheel gap and eliminating flow separation around the front wheel, the wheel fairing shows the most significant aerodynamic improvement. The rear wheel well shows a reasonable drag improvement, but since the tail of the bike acts almost as an enclosed wheel as it is, it is anticipated that the change in drag would be even greater if a similar device were used on the front wheel. Strangely, the wheel discs actually show an increase in drag, which could be an artifact of inadvertent rubbing. More tests will have to be performed to conclusively determine the impact of wheel discs. Based on the weight vs. drag table in Section 1.3 the front fairing and wheel well must weigh under 2.2 kg and 0.45 kg respectively to have a net benefit in the utility and speed event at the ASME race. Given that the parts weigh significantly less than this, they will both be employed in all race situations.

3.6 Steering damper

Objective: To improve handling qualities through the use of a steering spring/damper system.
Methodology: The handling characteristics of a streamlined vehicle are very important in determining the maximum achievable speed. In order to improve the handling of our previous vehicle, ACE, and thus design a better handling vehicle for 2011, a series of steering spring/damper systems were tested after ASME HPVC 2010. As seen in Figure 13 the spring/damper system consists of a rubber block that is deformed when the fork is rotated. The spring constant of the rubber block is 10 N/mm, and the steering stiffness depends how far the block is mounted relative to the steering axis. The steering damper was placed in two positions, 50 and 75 mm away from the steering axis. The rubber block was found to have an over-damped behaviour.
Results and Conclusions: Two sets of tests were conducted. A handling and controllability test meant to assess the steering spring/damper in tight, low speed manoeuvres, and a high speed stability test. The low speed test results are show below:

	No spring/damper	50mm offset	75mm offset
Minimum start velocity from which the vehicle is stable	2 m/s	1 m/s	0.8 m/s
Minimum radius turn a rider can hold comfortably	30 ft	20 ft	12 ft

The high speed tests were conducted on the 2 km long Downsview Airport runway, achieving speeds of more than 80 km/h. The results are shown below:

	No spring/damper	50mm offset	75mm offset
Maximum speed (four riders) km/h	69/NA/49/NA	80/82/74/59	78/80/70/54
Maximum comfortable side wind speeds	20 km/h	23 km/h	18 km/h

Overall four pilots were asked to evaluate the handling characteristics using the Cooper-Harper Handling Qualities Scale:

	No spring/damper	$50mm$ offset	$75mm$ offset
Cooper-Harper Rating (four pilots)	7/5/7/6	2/1/2/1	1/3/2/2

While the heavier damping and stiffer spring given by the larger offset allowed better low speed handling, the steering was heavy, and top speed slightly lower. All pilots considered the spring/damper to be highly beneficial, and we attribute the different Cooper-Harper ratings on individual preferences to the stiffness of the steering. The 50 mm offset steering was determined to be optimal and will be employed on the $Vortex$. Given that the ACE was able to achieve a Cooper-Harper Rating below 3, the team is confident that the $Vortex$ will meet design specifications for handling quality.

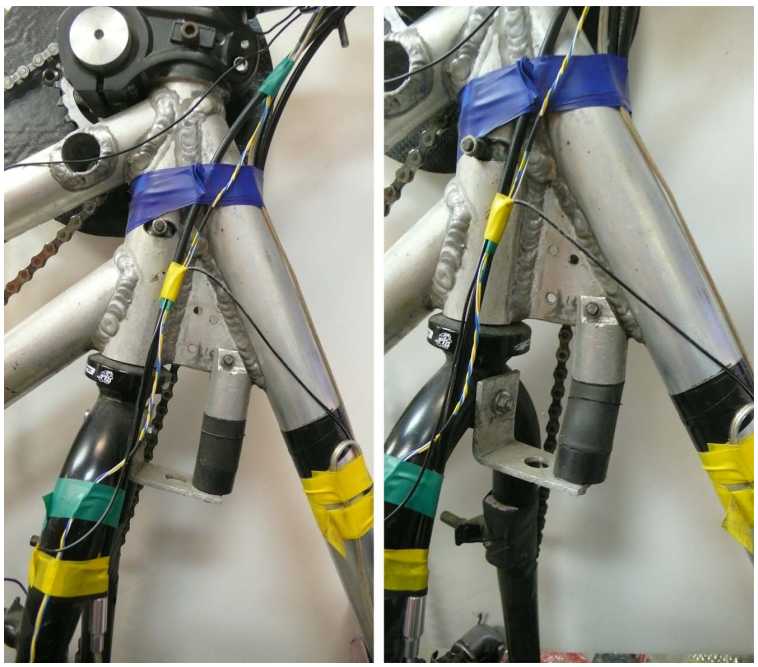

Figure 13: Rubber damper in the straight and turned position.

4 Practicality

4.1 Objective

The goal of the vehicle is to provide practical long range transportation, with no compromises made to its potential for high speeds. The specific utility objectives are: 24 hour riding, safe awareness of surroundings, ability to carry a varied amount of cargo, ease of transportation, ease of serviceability, the ability to ride in incremental weather, free-standing capability and protection against theft.

4.2 Environment

The vehicle is designed for Southern Ontario area around Toronto, where the University of Toronto is located. The city of Toronto is located in the province of Ontario, in the Great Lakes Lowland region of Canada (43°40-N, 79°24-W/O). It has one of the mildest climates in Canada[12]. Toronto is composed of a downtown core area, surrounded by boroughs. The population of Toronto is 2.48 million, and that of the Greater Toronto Area is 5.5 million. A diverse public transportation system exists (the Toronto Transit Commission), and is composed of an underground subway system, buses, streetcars, and light rail transit. During the busiest commuting times, 7-9am and 4-6pm, the system is quite crowded, making alternate commuting options desirable. A network of lit bicycle paths runs through Toronto and the Greater Toronto Area. These paths connect public parks and provide a safer, faster way for bicycles to move around. Many major streets also incorporate bicycle lanes or shared lanes in which drivers are made aware of bicycle traffic. These lanes are plowed and salted in the winter months to reduce snow coverage. A summary of relevant meteorological and climatic data from various sources [12, 2] is presented in the table below.

	Jan	Feb	Mar	Apr	May	Jun	Jul	Aug	Sep	Oct	Nov	Dec
Monthly avg temperature (°C)	-4.2	-3.2	1.3	7.6	14.2	19.2	22.2	21.3	17	10.6	4.8	-0.9
Days with temperature 0-30°C	14.4	14.1	24	29.4	30.5	28	25	28	29	31	28.5	20.8
Average total snowfall (cm)	31.1	22.1	19.2	5.7	0.1	0	0	0	0	0.5	7.6	29.2
Average total rainfall (mm)	24.9	22.3	36.7	62.4	72.4	74.2	74.4	79.6	77.5	63.4	62	34.7
Days with rainfall > 5mm	1.5	1.5	2.2	4.1	4.6	5.2	3.9	4.3	4.3	4	3.8	2.6
Average windspeed (km/h)	17.8	16.5	17.1	17.1	14.1	12.9	12.3	11.2	12.2	13.3	15.6	16
Average daylight hours (hr)	10.48	11.51	12.91	14.44	15.79	16.50	16.16	14.96	13.47	12.00	10.76	10.16

4.3 Ridable Hours per Day

The average number of daylight hours varies from 10.16 in December to 16.50 in June. Because Ontario observes Daylight Savings Time, normal work commuting times should fall within daylight hours. As described in the next section, the bike is fully equipped with the legally-necessary lights and reflectors for night-time riding, extending its rideable hours to 24 hrs/day.

4.4 Weather and Thermal days per year

As shown in the table above, there are a total of 303 days a year in which the temperature is between zero and 30°C. In addition, there 7 days per year in which more than five centimetres of

snow falls. Snow plows clear the snow from streets within a day, meaning that while it would be impossible to ride in fresh snow, it would be possible to ride the following day. Therefore, given that the temperature inside the cockpit generally stabilizes at 5° above the external temperature (see section on incremental weather), the total number of ridable days is 296.

4.5 Design Solutions

24 Hour Riding

By law in Ontario, bikes are required to have front facing white lights, rear facing red lights and reflective strips on the fork and seat stays. The white reflective strips, as well as the white forward light will be placed on the utility bar above the canopy as seen in Figure 14. The red rear facing light is placed in the trailing edge of the vehicle. In a racing situation, given that there is no need for lights, the Utility Bar can be easily disconnected from the bike.

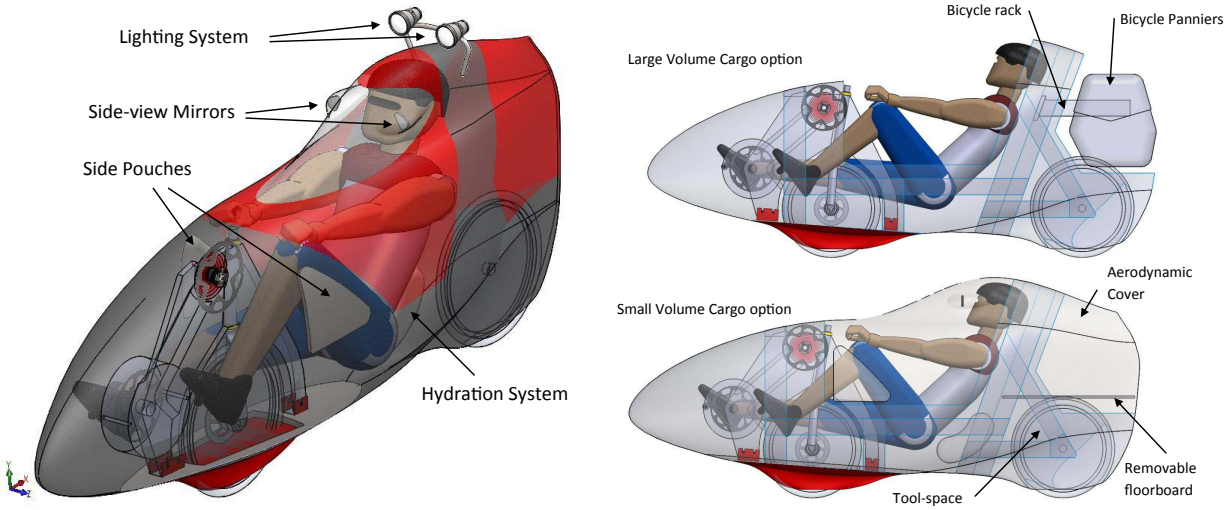

(a) (b)

Figure 14: Utility features of the *Vortex*.

Safe Awareness of Surroundings

The vehicle is designed to have an unobstructed 270° field of view, with special consideration paid to being able to see curbs and other road hazards. The figure below shows the field of view of the rider and how close he or she is able to see road hazards. In a turn, given that the bicycle is leaned in the direction of the turn, road hazards are much easier to see towards the inside of the turn. The vehicle will also have aerodynamically integrated rear-view mirrors. Two mirror arrangements were tested, the first consisting of a mirror located above the riders head, LeMans style, and the second consisting of traditionally placed mirrors on either side of the riders head. All three pilots tested

indicated that they prefer side mounted mirrors. In order to maintain aerodynamic efficiency, the mirrors are fitted inside the canopy, in aerodynamic pods, as seen in Figure 14.

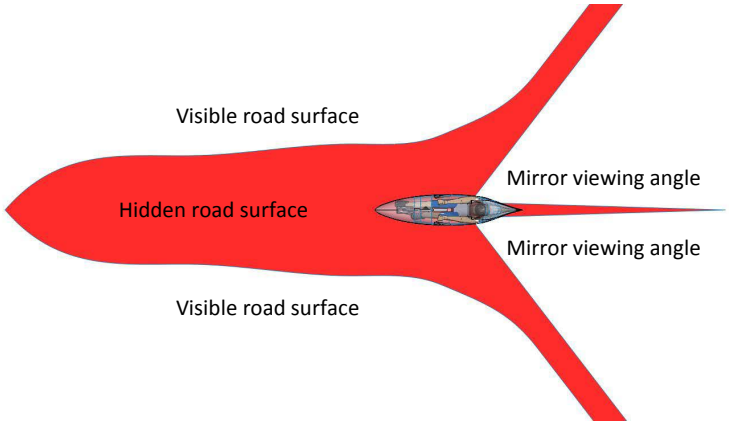

Cargo Capacity

The cargo systems of the vehicle consist of fixed and modular subsystems. There are two fixed cargo systems: the side pouches and the hydration system. The side pouches are made of a flexible mesh material. They are attached to the inside of the fairing in front of the door, and fit right under the riders arms in normal riding position, where they can be accessed while riding. They are intended for such accessories as wallets, cellphones, credit cards, keys or any other small item that cannot be carried on the riders person. The pouches are also located such that there is no contact between the body of the rider and the items stored in them. The hydration system consists of a Camelbak or similar water container stored under the riders seat, with a tube mounted such that the rider can drink without using their hands. Such a system was successfully tested during the 6 hour Black Bear endurance race in 2010 on the *ACE*. Both the pouches and the hydration system are shown in Figure 14. The main cargo carrying system is modular to allow the rider to choose between an aerodynamic, small volume cargo solution and a less aerodynamic, large volume cargo solution. As seen in Figure 14, the rear fairing is removable behind the roll cage, and provides space for 1 jug of water and 1 grocery bag above the rear wheel. A removable floor board allows access to the rear wheel if the cargo is removed. Left and right of the rear wheel well, below the floor board there is room for a pump and a set of bike maintenance tools. If a larger volume of cargo is needed, the rear fairing will be removed, and a rack system is bolted onto the shear wall. Regular cycling panniers can be mounted on this rack, allowing for increased cargo space. The time needed to change between the large and small cargo configurations is intended to be below 10 minutes.

Ease of Transportation

The bike is designed to be less than 8ft long, such that it fits inside a minivan without affecting driver visibility. The plug was tested inside a 2011 Dodge Caravan and fits with only one of the rear passenger seat folded. It allows the driver as well as two passengers (beside and behind the driver) to drive comfortably with space for luggage or tools.

Ease of Serviceability

All the mechanical systems of the bike, with the exception of the rear wheel and brake system, come attached to the Drivetrain Structure (see Figure 15). This structure can be removed entirely in several minutes with the quick release skewers, such that drive train maintenance can be performed outside the vehicle.

Incremental Weather Riding

The ability to ride in incremental weather depends on two issues: Water must be kept out of the bike and the temperature inside the bike must be maintained within acceptable ranges. The door of the vehicle has a flange system meant to ensure the correct alignment and rigidity of the structure. This system is also intended to seal the inside of the bike against rain or cold wind. Both wheels have wheel wells, to protect the rider from water sprayed by the tires. Additionally, the front wheel fairing protects the rider from cold air or water entering the wheel cut-out at most angles, and the remaining openings are sealed by a velcroed material. Finally, the ventilation system can be closed off from inside the vehicle, preventing water from coming in. All these features point to a very well insulated vehicle against rain and cold wind.

To regulate internal temperature an adjustable ventilation system is used, which was tested on the 2010 ACE as an addition for the World Human Powered Speed Championships. A screw is used to vary the opening of a NACA duct placed in front of the canopy, allowing it to be closed or opened as much as needed. With the NACA duct closed, temperature was measured inside ACE, with the rider pedalling inside. With an outside temperature of -1°C the temperature rose and stabilized at 5°C after roughly 10 minutes.

To allow the vehicle operation in hot weather, the air intake is very close to the riders face, enhancing breathing. Additionally, two cut-outs in the shear wall direct the air to the trailing edge openings, passing by the large veins in the riders neck, allowing for maximum cooling effect.

Free Standing Ability

In order to stop, start, enter, exit and park the vehicle without the help of additional personnel the $Vortex$ is equipped with a landing gear system, described in more detail in Section 3.4.

Theft Protection

Theft protection includes two aspects: the vehicle should be easy to lock and the vehicle should be easy to find in case of theft. Due to the shape of the vehicle, locking it to a common bike locking post is considered impractical, as it would block the sidewalk. The self contained locking system prevents the front wheel from turning with a skewer through the assembly. The key, as well as the removed skewer can be stored in the side pouches.

5 Safety

5.1 Normal operation

Safety systems designed for normal operation consider hazards that may be encountered by the rider in everyday situations. The following hazards were considered in the design:

- Pinch points: the chain is aligned along the centreline of the drivetrain assembly (far from the riders legs) and chain guards are installed on both sides of each sprocket. Chain guards prevent accidental pinching as well as chain derailment. Pinch points on the wheel are completely eliminated by using wheel wells which completely encapsulate the wheel.
- Sharp edges: interior features, including storage pockets, have been smoothed. Care has been taken in machining parts with smooth transitions. The steering tube ends are plugged to avoid injury to the rider while entering and exiting the vehicle.
- Visibility: 270 degrees of visibility is important in navigating traffic. Details of mirror placement used to achieve this are included in Section 4.5.
- Ventilation and hydration: rider comfort is key to safely handling the vehicle over long periods of time. Details of ventilation and hydration systems are included in Section 4.5.
- Night riding: a system of nighttime illumination has been developed to ensure visibility of the bike by other traffic after dark.
- Communication: a push-to-talk radio system allows riders to communicate during race situations. A cell phone can also be easily stored in the inside pockets and the vehicle has been tested to ensure that it is permeable to cellular signals.
- Steering system: the steering is directly bolted to the steerer using off the shelf components, thus ensuring proper installation.

5.2 Impact scenarios

Additional safety systems for racing and impact scenarios have been developed. The following systems have been incorporated for crash scenarios:

- Rollover/side protection system: The RPS is designed to fully protect the rider from crush and inertial forces imposed in crash situations. The rollcage can resist a 600 lb topload and 300lb sideload.
- Seat belt: a 4-point Sparco racing harness with a quick release buckle allows the rider to exit the vehicle quickly. If the rider is incapacitated, emergency personnel can also easily remove the harness.
- Door locking mechanism: in the case of a crash, the door will stay closed, protecting the rider inside. It is secured by two latches: one on each side of the rider. These latches are accessible from the outside of the bike as well, to access the rider if they become incapacitated.

References

[1] S. Black. Designing bicyclings lightest pro racing frame. http://www.compositesworld.com/articles/designing-bicyclings-lightest-pro-racing-frame, 2011.

[2] National Climate Data and Information Archive. Canadian climate normals 1971-2000, toronto, ontario. http://www.climate.weatheroffice.gc.ca/climate_normals/, 2011.

[3] M. Drela. Mark drela's quoted rules of thumb. www.recumbents.com/WISIL/barracuda/barracudafairingdesign.htm.

[4] M. Drela. Personal conversations with prof. drela. 2011.

[5] M. Drela and H. Youngren. XFOIL 6.9 user primer. http://web.mit.edu/drela/Public/web/xfoil/xfoil_doc.txt, Nov, 2001.

[6] G. Georgiev. Varna innovation and research corporation. www.varnahandcycles.com.

[7] P. Grant. *Course Notes: Human Control of Aerospace Systems*. University of Toronto, 2009.

[8] S. F. Hoerner. *Fluid-Dynamic Drag*. Hoerner Fluid Dynamics, Brick Town, N. J., USA, 1965.

[9] A. Jacobs. Velomobiel. en.velomobiel.nl/quest/technische_gegevens.php, 2011.

[10] A. Ligtvoet. Raptobike. www.raptobike.nl/, 2011.

[11] B. Moens. M5 ligfietsen and handbikes. www.m5-ligfietsen.nl/site/EN/Models/City_Racer/, 2011.

[12] National Research Council of Canada. Sunrise and sunset calculator. www.nrc-cnrc.gc.ca/eng/services/hia/sunrise-sunset.html, 2011.

[13] University of Toronto Human-Powered Vehicle Design Team. Design report: ACE human-powered speed vehicle. 2010.

[14] T. Ollinger. Streamliner scale sizing project. www.recumbents.com/wisil/scale_project/streamliners.htm, 2009.

[15] B. Patterson. *Lords of the Chainring, 5th Ed.* Cal Poly University, San Luis Obispo, CA, 2010.

[16] T. Reichert. Aerodynamic design of the vortex human-powered land-speed vehicle. 2011.

[17] S. Sanderson. Project sanderson. av-acg. http://www.flickr.com/photos/bhpclub/sets/72157604828238682/?page=1, 2009.

[18] A. Smith. Stratford's turbulent separation criteria for axially symmetric flows. *Journal of Applied Mathematics and Physics*, 28, 1977.

[19] G. Tamai. *The Leading Edge: Aerodynamic Design of Ultra-Streamlined Land Vehicles*. Bently Publishers, Cambridge, MA, USA, 1999.

[20] M. Weaver. Speed 101. www.speed101.com, 2003.

[21] D. Wielemaker. Varnowski aerodynamic data. www.recumbents.com/forums/topic.asp?TOPIC_ID=3672, 2010.

[22] D. Zolyniak. *Aerodynamic testing of the ACE human-powered land vehicle*. University of Toronto BASc Thesis, Ontario, Canada, 2011.

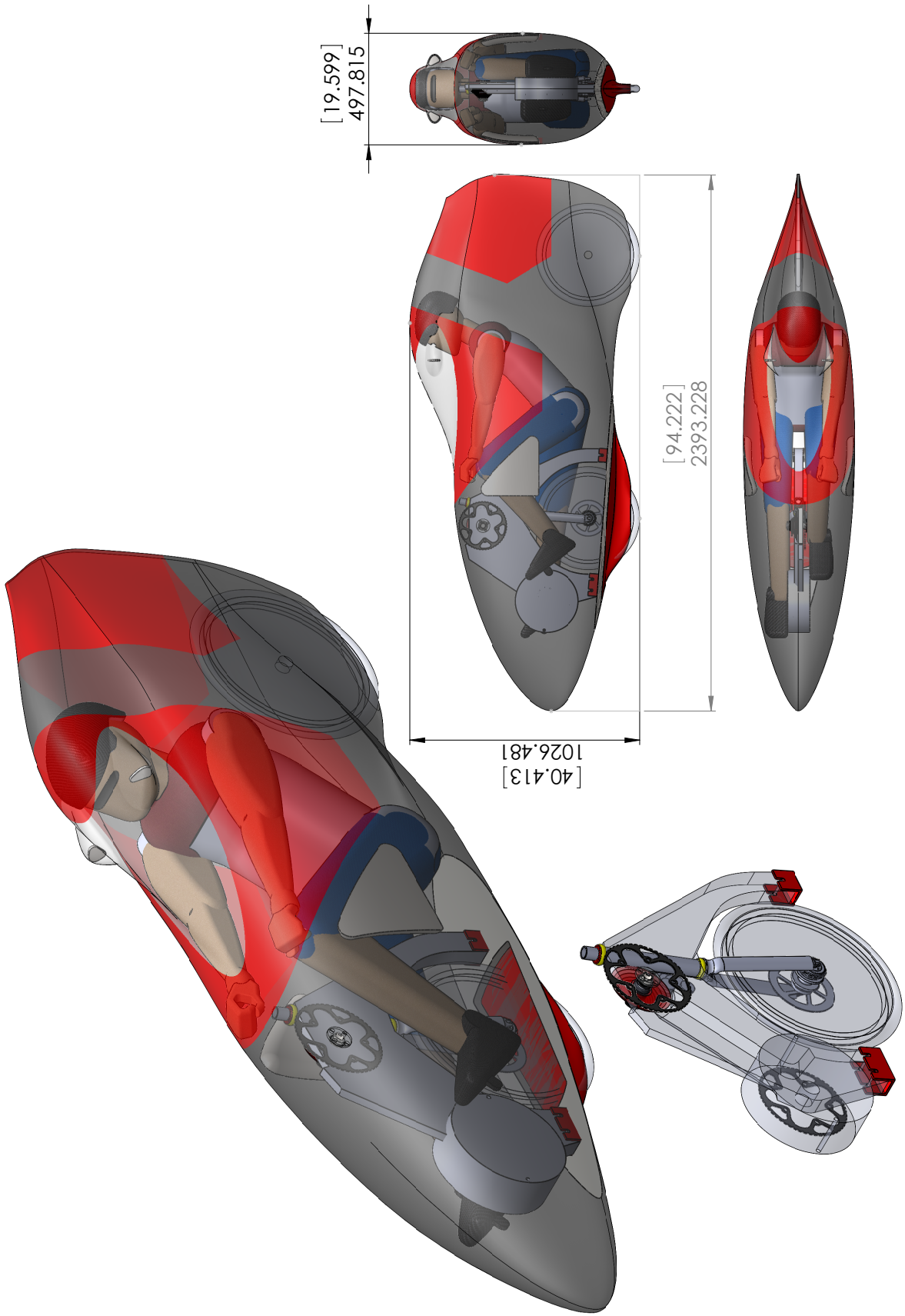

Figure 15: *Vortex* 3-View